Computer simulation of domain growth in ferroelectric liquid crystals

Joseph E. Maclennan, Qi Jiang, and Noel A. Clark
Condensed Matter Laboratory, Department of Physics, University of Colorado, Boulder, Colorado 80309
(Received 8 May 1995)

The electro-optic response of a surface-stabilized ferroelectric liquid crystal (SSFLC) cell is determined largely by the dynamics of polarization reversal at the chevron interface. This process involves the nucleation, growth, and ultimate coalescence of polarization reversal domains. These domains are generally faceted, being either polygonal or characteristically boat shaped. We have performed computer simulations in two dimensions (2D) of field-driven domain growth at the chevron interface in SSFLCs. By including elastic anisotropy and the orientational binding of the chevron in the equation of motion, we get anisotropic domain growth and, for a range of applied field strengths E, partially faceted domain shapes. The measured growth rates have the same field dependence as is seen experimentally, the domain area increasing as $A \propto (Et)^2$. We have also developed an analytical algorithm similar to the Wulff construction for calculating the spatial evolution of 2D domains as a function of time for arbitrary starting shapes. In the present case of ferroelectric domain growth, we can derive full 2D domain shapes with curved walls from the directional variation of the velocity of planar walls as measured by computer simulations in only 1D.

PACS number(s): 61.30.Cz, 61.30.Gd, 83.70.Jr, 77.80.Fm

I. INTRODUCTION

Chiral molecules in any tilted smectic liquid crystal phase are ferroelectric, with a spontaneous polarization $\mathbf{P}$ oriented perpendicular to both the layer normal $\hat{\mathbf{z}}$, and the molecular director $\hat{\mathbf{n}}$ [1]. The director is tilted from the layer normal by a temperature-dependent angle ψ_0 (typically $\sim 20°$) and the azimuthal orientation of the polarization is given by $\phi(\mathbf{r})$. When prepared in the smectic-C (Sm-C) phase with the layers oriented more or less perpendicular to closely spaced, conductive bounding plates (the "surface-stabilized" geometry), such materials form the basis of fast electro-optic devices [2].

The optical response of these surface-stabilized ferroelectric liquid crystals (SSFLCs) is in general a complex function of the cell thickness, the chemistry of the cell surfaces, and the material parameters of the liquid crystal itself. In cells with chevron layer structure (as sketched in Fig. 1), the chevron interface (which is typically near the midplane of the cell) provides an additional internal surface with an associated orientational energy anisotropy that controls the director orientation in the interior of the cell [3].

The direction of the ferroelectric polarization at the chevron interface can be switched between up and down by relatively weak fields ($E \sim$ a few V/μm) [4,5]. Since the molecules in the rest of the cell are elastically coupled to those at the chevron interface, this in turn induces a reorientation in the bulk that results in a net change in the average optical axis orientation of the cell. When the cell is suitably oriented between crossed polarizers, this causes a large change in the optical transmission. Further increasing the applied field ($E \gtrsim 10$ V/μm) causes any hitherto unswitched cell surface to reorient also, resulting in a small additional change in transmission.

The optical response of many SSFLCs is thus determined primarily by the switching at the chevron interface [5]. This process typically involves the nucleation and subsequent growth of many individual, switched domains of high optical contrast. In the two-dimensional (2D) view afforded by the polarizing microscope, these domains are polygonal in low applied fields and become almost elliptical in high fields [6,7]. Some typical domain shapes are shown in Fig. 2. Understanding the dynamics of the nucleation and growth of these domains is an important part of being able to model and predict the electro-optic response of chevron SSFLC devices.

In this paper, we present a 2D model of domain growth at the chevron interface. The key features of this model are the explicit inclusion of a chevron potential (which prevents director reorientation except at domain boundaries) and of elastic anisotropy (which results in anisotropic growth). Numerical solution of the equation of motion for this system allows us to model the temporal evolution of switched domains as a function of applied field. When the equation of motion is reduced to 1D and solved in an anisotropic space, we can recreate 2D domain shapes by implementing a mathematical algorithm analogous to the Wulff construction used to find the equilibrium shapes of crystals. We can compare the calculated forms and growth rates of model domains with those observed in SSFLC cells. The results indicate that the ferroelectric Sm-C phase is of lower symmetry than the model employed here. However, they also show that 3D domain shapes with curved walls can be obtained by combining the results of 1D or 2D simulations of planar walls in a 3D liquid crystal medium.

In Sec. II we will summarize the basic experimental observations on switching in chevron SSFLCs to date. In Sec. III we present a theoretical description of direc-

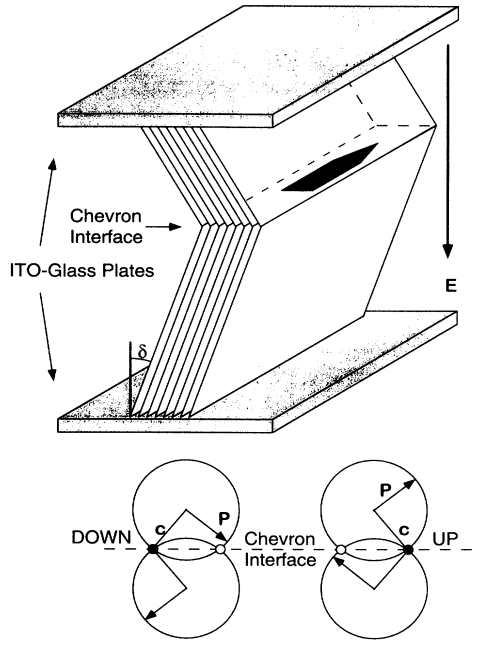

FIG. 1. Geometry of chevron SSFLC cell. The smectic layers are tilted an angle $\pm\delta$ from the cell normal, the change in their orientation typically occurring near the middle of the cell. The orientational binding potential at this planar chevron interface stabilizes two polarization states **P**, up and down. The corresponding director orientations are indicated in the lower part of the figure by the filled circles (•) and their projections onto the smectic layer planes by the c director (**c**). A generic polygonal domain is shown growing at the chevron interface.

tor orientation dynamics in SSFLCs and motivate a particular 2D formulation applicable to chevron cells. We then show that the equation of motion can be reduced to 1D for the case of planar domain walls and illustrate, in Sec. IV, how 1D solutions along discrete directions in space can be combined to recreate complete 2D domain shapes. The results of selected simulations are presented in Sec. V, for both the 2D and 1D models. We conclude in Sec. VI by comparing the domain growth in our model system with that observed experimentally.

II. EXPERIMENTAL BACKGROUND

The morphology of ferroelectric domains in high-speed switching experiments was first observed by Handschy and Clark using stroboscopic microscopy [6]. They reported seeing approximately elliptical domains extended along the layer direction, whose growth they originally attributed to switching at the cell surfaces [8]. Ouchi *et al.* pointed out that slow voltage ramps generate domains which grow with characteristically asymmetric "speedboat" forms. On the basis of microscopic observations of nonuniform states in SSFLCs, they also proposed that the domain walls were director field disclinations located in the interior of the cell rather than at the bounding glass plates [9]. The origin of these disclinations was not understood at that time.

Early 2D numerical simulations of director reorientation based on Handschy and Clark's model were carried out by Nonaka *et al.* [10] and by Yamada *et al.* [11]. By considering ferroelectric dipoles arranged in a sheet oriented perpendicular to the glass plates of their model

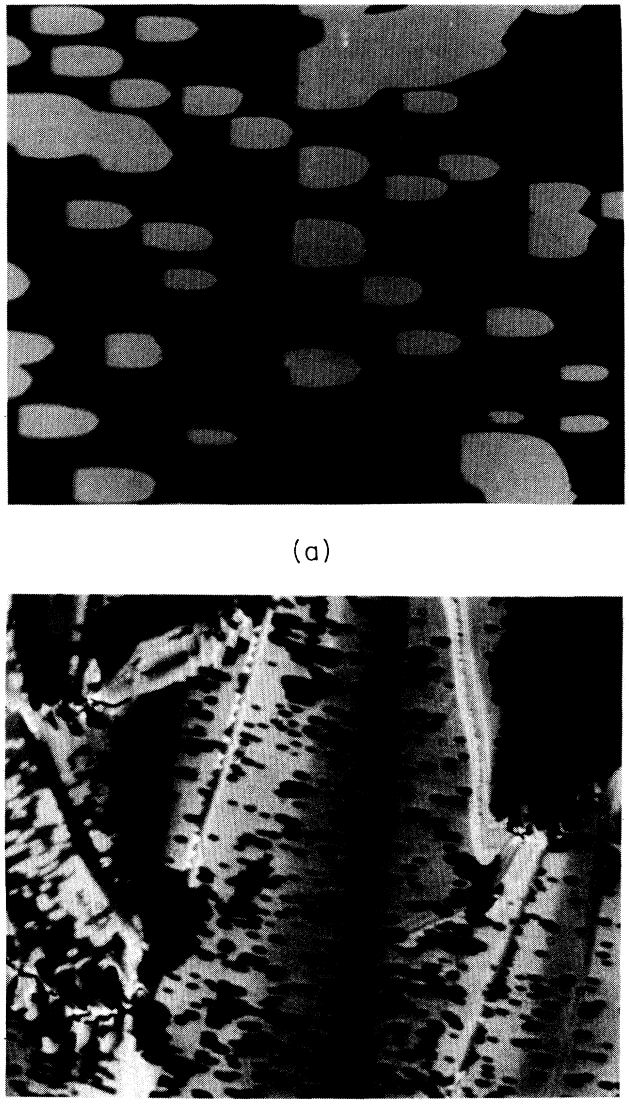

FIG. 2. Domain shapes in chevron SSFLC cells: (a) low-voltage switching in a 4 μm cell of the Merck material ZLI-3654. The domains are boat shaped, with gently rounded sides. The applied voltage is about 20 mV. (b) High-voltage switching in a 2 μm cell of the Displaytech mixture W7-W82. The picture, taken stroboscopically, shows rather symmetric domains growing about 3 ms after a field reversal. The applied voltage is 12 V. The layer normal is in both cases approximately vertical.

cell, they were able to simulate the growth of surface domains in cells with bookshelf layer geometry. Ishibashi and co-workers also made stroboscopic measurements of switching in SSFLC cells and analyzed the nucleation and growth of domains using the Avrami model [12].

After the discovery of chevron layer structure in SSFLCs [3], it was realized that the low-voltage switching which gives rise to boat domains, and which is in fact responsible for the main change in optical transmission in these cells, was due to director reorientation *at the chevron interface.* In a model which reconciled their x-ray data with Ouchi's optical observations, Clark and Rieker proposed that the molecular orientation at the chevron interface is controlled by a surface potential that minimizes changes in the director orientation across this interface [13]. This internal boundary condition is satisfied in a typical cell when the director at the chevron interface is oriented parallel to the interface (and hence also parallel to the bounding glass plates). Since this condition is met at two different positions on the Sm-C tilt cone, SSFLCs in the absence of applied field support two distinct, coexisting polarization states, which we call "up" and "down." The geometry of chevron cells is shown in Fig. 1.

It was originally pointed out by Ouchi *et al.* that boat domains growing on opposite sides of a "zigzag" wall point in opposite directions [9]. It is now firmly established that zigzag defects serve to invert the direction of the chevron [13] and that the boat domains form during a field-driven transition between two stable, nonuniform director states, "(half-splayed) up" and "(half-splayed) down" [4]. The present model of chevron switching is illustrated in Fig. 3, which shows a SSFLC cell in which a down domain, in which the director field above the chevron interface is uniform and that below splayed, is growing in an up environment. Optical transmission spectrometry experiments have confirmed that in typical SSFLC cells the low-voltage chevron switching accounts for most of the obtainable contrast, the additional change in transmission obtained by increasing the electric field enough to reorient one of the cell surfaces being relatively small [5].

Further high-speed stroboscopic measurements of domain nucleation and growth dynamics in chevron SSFLCs were recently reported by Xue and Clark [7]. Their experiments studied the crossover from "heterogeneous" (defect-generated, repeatable) nucleation at low voltages to "homogeneous" (spatially random) nucleation at higher voltages originally observed by Handschy and Clark [6]. They measured the growth dynamics at different temperatures and confirmed that the mean size of any domain increases approximately linearly with time ($\langle d \rangle \propto t$), and that the domain wall velocity is linear in the applied field ($v \propto E$) and is constant in time. They found that the "boat" domains are typically irregular hexagons or pentagons extended along the smectic layers, whose front-back ("bow-stern") asymmetry is reduced with increasing field strength. They also suggested that electro-hydrodynamic backflow effects might account for this asymmetry.

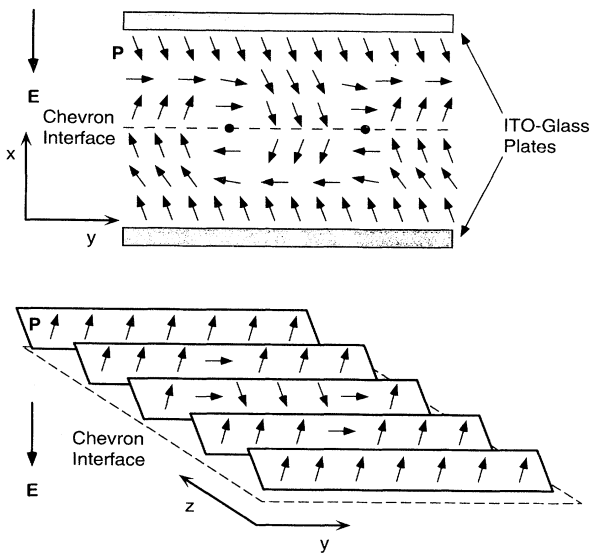

FIG. 3. Domain switching at the chevron interface. A down domain is shown growing in an up environment, the arrows representing the polarization field **P**. The upper diagram is a transverse view of the cell with the chevron domain boundaries indicated by filled circles (•). The lower diagram shows a cut through the tilted smectic layers just above the chevron interface. This is the 2D space modeled in the numerical simulations.

III. THEORY

The dynamics of director reorientation in SSFLC cells can be described by the equation of motion derived from an appropriate Landau–de Gennes free-energy functional [8]. For a uniformly layered ferroelectric liquid crystal, the free-energy density f may (if we ignore flow effects) be written

$$f = \frac{K_{BS}}{2}(\nabla_{xy}\phi)^2 + \frac{K_T}{2}(\nabla_z\phi - q)^2 \pm PE\cos\delta\cos\phi - [\Delta\epsilon E^2 \sin^2(\psi_0)/8\pi]\sin^2\phi - \frac{\gamma_4}{\ell}\cos\chi, \quad (1)$$

where K_{BS} and K_T are the Frank elastic constants for distortions of the director field, respectively, within and normal to the smectic layers (i.e., bend-splay vs twist of **P**), $\Delta\epsilon$ is the dielectric anisotropy, q is the wave vector of the spontaneous ferroelectric helix, and δ is the smectic layer tilt angle.

The last term describes orientational binding at the chevron interface: γ_4 has the dimensions of a surface energy anisotropy per unit area, and ℓ denotes the decay length of the orientational binding potential. χ is the angle subtended between the directors immediately above and below the chevron interface [13], with χ given implicitly by

$$\cos\chi = \cos 2\delta \cos^2\psi_0 + \sin 2\delta \sin\psi_0 \cos(\psi_0)(\sin\phi_+ - \sin\phi_-) + \cos 2\delta \sin^2\psi_0 \sin\phi_+ \sin\phi_- + \sin^2\psi_0 \cos\phi_+ \cos\phi_- \ .$$

The angles ϕ_+ and ϕ_- refer to the polarization azimuth, respectively, just above and just below the chevron interface. Earlier numerical solutions of reorientation in chevron SSFLCs performed in 1D (along the cell normal) [4] showed that when the molecules on either side of the chevron interface reorient in an applied field, they always remain mirror images of each other, i.e., $\phi_+ = -\phi_-$. This means that the angle χ can be determined uniquely from the director orientation ϕ on one side of the interface only. The chevron binding potential then has the shape shown in Fig. 4, with the minima corresponding to the up and down states satisfying $\sin\phi = \tan(\delta)/\tan\psi_0$. For a smectic tilt angle $\psi_0 = 22°$ and layer tilt $\delta = 18°$, the equilibrium polarization orientations at zero field are $\phi \approx 54°$ and $\phi \approx 126°$.

In the ferroelectric ($\pm PE\cos\phi$) term, the + sign means the field favors an up orientation ($\phi = \pi$) and − favors down ($\phi = 0$). We have neglected variations in the tilt angle, flexoelectricity, the self-field of the ferroelectric polarization, and inertial effects. The applicability of these approximations is discussed elsewhere [8,14,15].

Variation of Eq. (1) gives the equation of motion, which, with the inclusion of a viscosity η that damps azimuthal motion of the director on the tilt cone, is

$$\eta\phi_t = K_{BS}(\phi_{xx} + \phi_{yy}) + K_T\phi_{zz} \pm PE\cos\delta\sin\phi + [\Delta\epsilon E^2 \sin^2(\psi_0)/4\pi]\sin\phi\cos\phi - \frac{\gamma_4}{\ell}\frac{\partial}{\partial\phi}\cos\chi. \quad (2)$$

We have sought in the present work to simulate and understand the domain growth dynamics observed in the stroboscopic experiments. Although a complete description of chevron switching would necessarily involve a 3D model, we treat the director field as two dimensional in the plane of the chevron interface. The motivation for this can be seen from Fig. 3. Here a down field has been applied to a down domain nucleated at the chevron interface. Only the molecules at the chevron interface switch because the polar interactions at the solid-FLC interface are too strong to allow switching there. Once the director has switched at the chevron interface, three regions can be distinguished: mostly down, mostly up, and the walls. In the nonequilibrium steady state, these structures are internally time independent, with the walls moving to increase the down area. This problem can be viewed as effectively 2D, with the field variable being the director orientation on the chevron interface. In this case, where the applied electric field is strong enough to switch the polarization at the chevron interface but not at the cell surfaces, the optical transmission of the SSFLC cell is dominated by the orientation at the chevron interface.

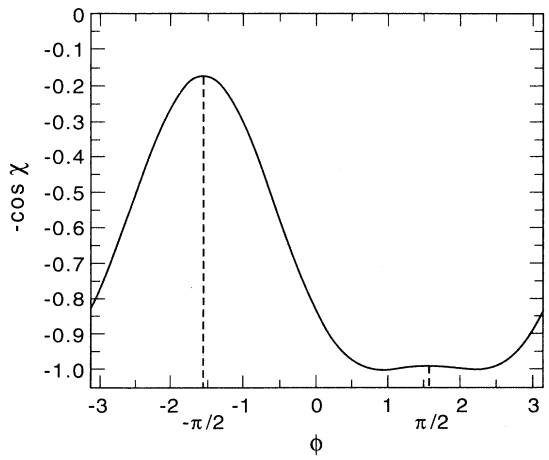

FIG. 4. Chevron binding potential ($W_4 \sim -\cos\chi$). The energy minima corresponding to the down and up polarization states are located symmetrically about $\phi = \pi/2$.

We therefore ignore director field variations in the $\hat{\mathbf{x}}$ (cell-normal) direction and consider a 2D dipole sheet in the y-z plane, centered on the chevron interface. We assume that the chevron is in the midplane of a cell of thickness d and further simplify the problem by considering the orientation just above the chevron interface only.

Letting $\phi_{xx} = 0$, if we divide Eq. (2) throughout by PE, and scale time by $\tau = \eta/PE$ and distance by the correlation length $\xi = (K_{BS}/PE)^{1/2}$, we obtain the dimensionless equation

$$\phi_t = \phi_{yy} + \frac{K_T}{K_{BS}}\phi_{zz} \pm \cos\delta\sin\phi + \alpha\sin\phi\cos\phi - \lambda_4\frac{\partial}{\partial\phi}\cos\chi\ , \quad (3)$$

where $y/\xi \to y$, $z/\xi \to z$, and $\lambda_4 = \gamma_4/(\ell PE)$. The dielectric interaction strength scales with $\alpha = [\Delta\epsilon E\sin^2(\psi_0)/4\pi P]$: for the moderate field strengths considered in our simulations, however, the dielectric contribution would be negligible and so we shall omit it entirely, setting $\alpha = 0$.

The ϕ dependence of the chevron term is given explicitly by

$$\frac{\partial}{\partial\phi}\cos\chi = \sin 2\delta \sin 2\psi_0 \cos\phi - (\cos 2\delta + 1)\sin^2\psi_0 \sin 2\phi\ .$$

It is evident from this expression that Eq. (3) can *not* be reduced to the form of a diffusive (double) sine-Gordon equation, which precludes an easy prediction of the domain wall dynamics in this system [15]. In the absence of an electric field, the up and down polarization states are equally stable. In a down applied field, dipoles in both states are affected by an electrical torque and tend to align more closely with the field. When switching occurs via domain growth, the up state directors are prevented from reorienting *en masse* by the chevron binding potential and reorientation can only be mediated by the motion of domain walls. Only in electric fields large enough to overcome the binding potential directly would we expect a homogeneous reorientation of the director field that requires no domain wall motion.

Finally, we note that the elastic anisotropy inherent in

the equation of motion can be parametrized in terms of an angle β describing a set of axes (v, w) rotated from (y, z), to yield the equation

$$\begin{aligned}\phi_t = &\left(\sin^2\beta + \frac{K_T}{K_{BS}}\cos^2\beta\right)\phi_{ww} \\ &+ \sin(2\beta)\left(\frac{K_T}{K_{BS}} - 1\right)\phi_{vw} \\ &+ \left(\cos^2\beta + \frac{K_T}{K_{BS}}\sin^2\beta\right)\phi_{vv} \\ &\pm \sin\phi\cos\delta - \lambda_4\frac{\partial}{\partial\phi}\cos\chi\,. \end{aligned} \tag{4}$$

This formulation allows us to solve the 2D equation of motion for the special case of a 1D domain wall propagating along an arbitrary direction in the y-z plane (e.g., along the v axis, so that $\phi_{vw} = \phi_{ww} \equiv 0$).

We see from Eq. (4) that the growth of ferroelectric domains in our model should depend on two parameters only: (1) the ratio of the Frank elastic constants K_T/K_{BS} and (2) the ratio of chevron to electrical potential energy given by λ_4.

The decay length of the chevron potential is set in our simulations to $\ell = \min[\xi, d/2]$, so that the chevron binding acts in a slab of effective thickness ℓ that increases with decreasing field strength but can never exceed $d/2$.

We have chosen to explore two complementary approaches to simulating domain growth in SSFLCs. First, we have performed simulations in 2D by solving Eq. (3), which enables us to observe directly the evolution of a single domain for a variety of initial starting shapes and applied field strengths. Second, we have numerically solved the 1D Eq. (4) to find the steady-state profile and wave speed $v(\beta)$ of a planar up-down domain wall as a function of its orientation. We have developed a general mathematical algorithm analogous to the Wulff construction method of deriving crystal shapes from the polar plots of surface energies that allows us to calculate steady-state 2D LC domain shapes from the composite 1D velocity profile $v(\beta)$. The formalism is summarized in the following section.

We approximated Eqs. (3) and (4) using the semi-implicit Crank-Nicholson finite difference scheme, with the integrations in time being performed in alternating directions [16]. Elastic boundary conditions were imposed [8]. We typically used 101×101 mesh points in 2D and 151 mesh points for the 1D simulations, which were carried out on Silicon Graphics computers. The simulation results appear in Sec. V.

IV. DYNAMIC DOMAIN SHAPE CALCULATION

The problem of determining the equilibrium shape of a crystal growing in 2D is classic. Early this century, Wulff [17] developed a geometric construction that gives the equilibrium shape of crystals with known surface tension anisotropy, $\gamma(\beta)$. Facets in the crystal shape correspond to directions of local minima in $\gamma(\beta)$. Crystals for which $\gamma(\beta)$ contains several, sufficiently deep minima may end up being entirely faceted (i.e., polygonal). Herring pointed out that even liquid crystals with no positional order but possessing orientational order could exhibit domain shapes with sharp edges or corners [18]. Recently, Rudnick and Bruinsma have developed a formalism for calculating domain shapes of liquid-crystal-like systems when the total energy depends not only on the surface orientations but also on the internal structure of the domain [19]. They find that when the internal structure is described by a 2D XY model then cusps ought to be a generic feature of the resulting domain shapes.

We have developed a general algorithm for calculating the steady-state shape of domains using the normal velocity profile $v_\perp(\beta)$ of the domain boundaries rather than the surface energy. The analysis is consistent with the experimental observation that the mean dimension of any domain in chevron cells increases linearly with time [7]. This implies that under equilibrium growth conditions the domain shape at an arbitrary time t_3 is geometrically similar to the shape at any earlier times t_1 or t_2. The location of the domain boundary is therefore given by the relation

$$r(\theta, t) = v(\theta)t\,, \tag{5}$$

where θ is the angle between $\hat{\mathbf{r}}$ and the y axis as shown in Fig. 5. Under conditions of stable growth, the velocity profile $v_\perp(\beta)$ is independent of time and the domain wall velocity $v(\theta)$ is independent of r along any given direction.

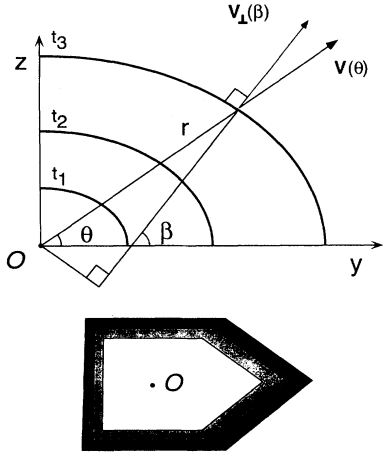

FIG. 5. Geometry of domain shape calculations. Part of a curved domain wall $r(\theta)$ is shown at different times t_1, t_2, and t_3. The radial domain wall velocity $v(\theta)$ is constant for a given θ. The local orientation of the domain wall along any radius vector is also constant in time so that the growth is self-similar. The construction relates the radial velocity to the normal component of the velocity $v_\perp(\beta)$, the latter being equal to the velocity of an infinite planar wall with the same orientation. The lower part of the figure shows a hypothetical five-sided boat domain growing in self-similar fashion: the pointed bow moves fastest and is furthest from the "origin" O.

We will show that if we know $v_\perp(\beta)$ for any given system, we can find the equilibrium domain shape using Eq. (5). We can see, from the geometric construction in Fig. 5, that the radial growth velocity has the form

$$v(\theta) = \frac{v_\perp(\beta)}{\cos(\beta - \theta)} . \tag{6}$$

When $v_\perp(\beta)$ is known, the domain shape problem reduces to finding the angle θ as a function of β. This can be done in a straightforward way. Rather than performing a conventional Euler-Lagrange minimization of the free energy [17–19], we perform partial differentiations of Eq. (6), which yield

$$\frac{1}{v_\perp(\beta)} \frac{\partial v_\perp(\beta)}{\partial \beta} = -\tan(\beta - \theta), \tag{7a}$$

$$\frac{1}{v(\theta)} \frac{\partial v(\theta)}{\partial \theta} = -\tan(\beta - \theta) . \tag{7b}$$

Combining Eqs. (5)–(7) enables us to calculate stable domain shapes from $v_\perp(\beta)$. An extension of the method to the case of non-steady-state growth also allows us to compute the domain shape as a function of time for arbitrary starting shapes [20]. The method is quite general and applies both to conventional crystal growth and to liquid-crystal domain evolution.

We have used the 1D velocity profiles for ferroelectric domain growth determined by solving Eq. (4) to compute the expected 2D equilibrium shapes. The velocity profiles were typically calculated at 10° intervals in β, with intermediate values being found by polynomial interpolation. The shapes obtained in this way were compared with those obtained in the full 2D simulations for a range of experimental parameters and found to be in good agreement. Examples will be shown in the next section.

V. RESULTS

We have solved the 2D Eq. (3) for the case of a small down domain in an up environment, growing in an applied electric field. The system is well behaved, in the sense that the asymptotic form of the growing domain does not depend on its initial shape. For any given set of physical parameters, both polygonal and elliptical domain nuclei with either smooth or rough boundaries all evolve within a few characteristic times τ to the same smooth, generally elongated shape.

Assigning different values of the elastic constants K_T and K_{BS} to the twist and bend-splay distortions of $\mathbf{P}$, in accord with what is known of Sm-C phases, is found to be an essential condition for generating anisotropic growth in the y-z plane. In addition, our simulations are the first to produce partial faceting similar to what is observed experimentally.

Faceting in this model is a combined consequence of the elastic anisotropy and the chevron potential. The domain wall velocity is smaller along the layer normal $\hat{\mathbf{z}}$ than along the layers themselves because $K_T < K_{BS}$. The chevron binding term introduces an energy barrier that further slows down wall motion, causing a pronounced cusp in the velocity diagram at $\beta = 90°$ that is in turn responsible for faceting. There are no facets in the absence of the chevron term. Figure 6 shows examples of domain shapes and velocity profiles for different values of the elastic constants and chevron potential.

The evolution of the system depends in a complex way on applied field strength E, the elastic constants K_T and K_{BS}, and the chevron anchoring strength γ_4. By varying the values of K_T/K_{BS} and λ_4 we have established the phase diagram for domain growth in chevron SSFLCs

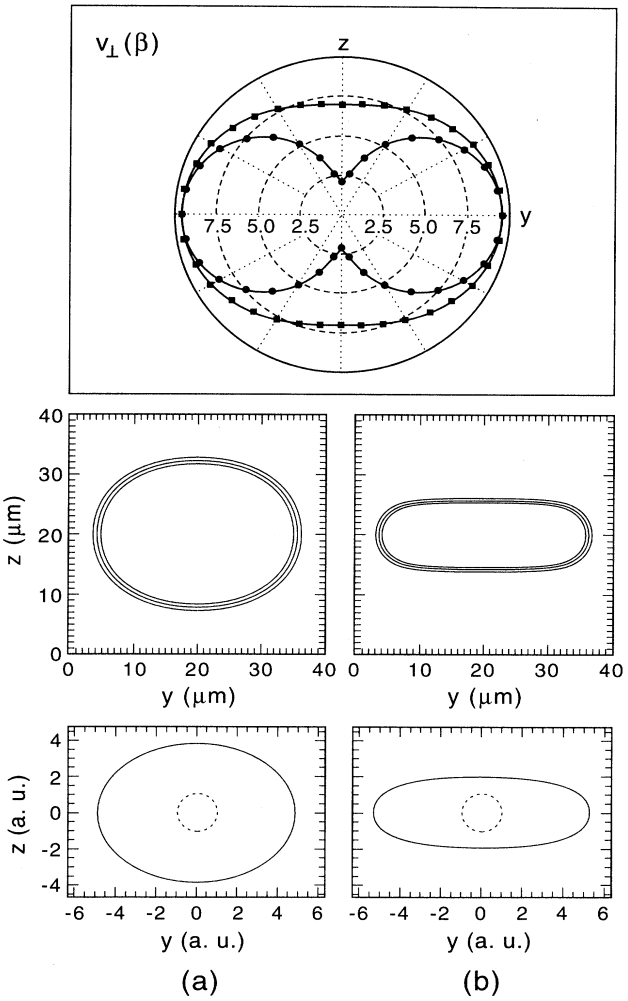

FIG. 6. Ferroelectric domain shapes in 2D. The figure shows normal velocity profiles $v(\beta)$ and steady-state domain shapes for two different ratios of the elastic constants, $K_T/K_{BS} = 3/5$ (■) and $K_T/K_{BS} = 1/5$ (•). The upper pair of domain shapes is the result of full 2D simulations, while the lower pair is computed (in arbitrary units) from the 1D velocity profiles $v(\beta)$ assuming the domains are initially circular (dashed curves). For the trivial case when the elastic constants are equal, the domain shape and velocity profile are perfectly circular. The velocities are in μm/ms, and the 2D contours are plotted for $\phi = 1$, 1.5, and 2 radians.

shown in Fig. 7. We can identify three distinct regions of parameter space in this diagram.

(1) In *moderate* electric fields (region B), there is anisotropic domain growth mediated by the motion of solitonlike domain walls. The sides of the domains (parallel to the smectic layers) are well-defined facets. The domains grow equally fast along $+\hat{\mathbf{y}}$ and $-\hat{\mathbf{y}}$ and have rounded ends. The domain shape varies from elliptical to cigar shaped.

(2) In *large* electric fields (region A), the ferroelectric coupling is big enough to overcome the chevron energy barrier everywhere in the sample. While there is initially some identifiable wall motion at the domain boundary, the surrounding up region reorients in a homogeneous manner at the same time and the entire sample is soon switched to the down state, with no remaining trace of any domain structure.

(3) In *small* applied electric fields (region C), the initial domain does not grow but shrinks instead. We will show in Sec. VI A that this is a consequence of the elastic energy stored in the curved domain walls, which acts as an effective surface tension opposing any expansion of the domain: below a certain threshold field E_{th} domains do not grow, while above E_{th} they should, in principle, grow without limit.

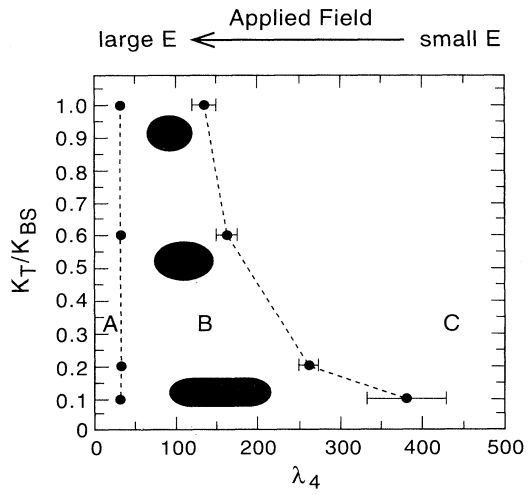

FIG. 7. Model phase diagram for 2D domain growth in chevron SSFLCs. This figure summarizes the behavior of a down domain of initial radius $R = 12$ μm nucleated in a sheet of up dipoles. In sufficiently high fields (region A), the electrical torques are strong enough to overcome the chevron binding potential everywhere in the sample and the polarization in the up region switches homogeneously. In very low fields (region C), the electrostatic torques are overcome by elastic torques tending to minimize the length of the domain boundary, causing the domains to shrink and vanish. At intermediate field values, the steady-state domain shape becomes more elongated as the elastic constants are made more anisotropic, and more faceted as the chevron potential strength γ_4/ℓ is increased. The dashed line at the B-C boundary is intended as a guide to the eye. The error bars for the A-B boundary would be smaller than the plotted symbols.

As an alternative to performing full-blown numerical simulations in 2D, we have also constructed domain shapes from the 1D velocity profile as explained in Sec. IV above. These shapes are in good qualitative agreement with the 2D results, as can be seen in Fig. 6.

In addition, we have solved Eq. (4) to find the 1D domain wall velocity as a function of applied field (the other model parameters being held fixed). The results are plotted in Fig. 8, which shows that this dependence is approximately linear ($v_\perp \propto E$), in agreement with the measurements of Handschy and Clark [6] and Xue and Clark [7]. This result is markedly different from the case of a 1D damped sine-Gordon wave propagating between $\phi = 0$ and $\phi = \pi$, where the wave speed $c^* \propto \sqrt{E}$ [15]. The inclusion of the chevron binding potential in Eq. (1) thus has a fundamental effect on the speed of solitary waves. We are not aware of any analytical predictions of the wave speed for this particular variant of the sine-Gordon equation.

Although the velocity dependence in Fig. 8 is proportional to E on the average, it is clear that the curve has two distinct regions: below a critical field $E_c \sim 0.25$ V/μm, the dependence is strictly linear ($v_\perp \propto E$), while above E_c it is not. The two regions of Fig. 8 arise mechanically because of how the effective chevron torque is evaluated in the simulations. As we explained in Sec. III, the chevron potential effectively acts over a distance ℓ above the chevron interface. For moderate and large applied fields, we set $\ell = \xi \equiv (K_{BS}/PE)^{1/2}$, the electric field correlation length. At fields below the critical value $E_c = 4K_{BS}/(d^2P)$, we have $\xi > d/2$ and so we need to impose a physical cutoff at $\ell = d/2$ for all $E < E_c$. Thus the chevron potential acts in a kind of virtual slab which has fixed thickness below E_c and ever decreasing thickness above E_c. For $E > E_c$, the calcu-

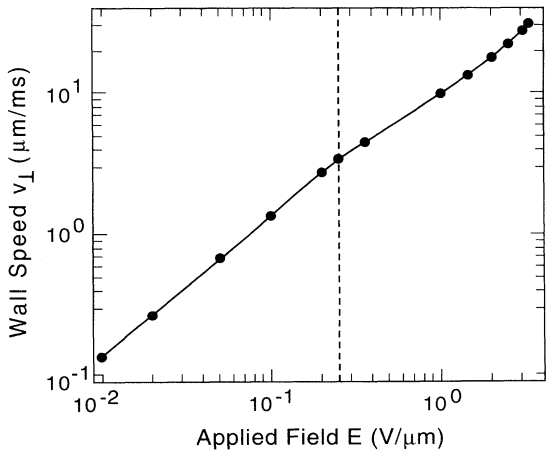

FIG. 8. Plot showing the velocity $v_\perp$ of a planar chevron domain wall as a function of applied electric field strength E. The dependence is approximately linear ($v_\perp \propto E$). The dashed line delineates the field strength for which $\xi = d/2$, as discussed in the text. Logarithmic axes are used to distinguish more clearly the low and high field regions.

lated velocity curve is superlinear. We note that in the data of Xue and Clark [7] there are also indications of curve steepening with increasing E, although the sparsity of their experimental data points makes a systematic comparison difficult.

Finally, we point out that the 1D simulations can only be used to reproduce part of the 2D phase diagram of Fig. 7. This is because while there is a critical field above which a 1D solitary wave will collapse, just as in the 2D case, there is no mimimum field for growth in 1D: the electrical potential energy of the system is lowered in both 1D and 2D if the field-favored region grows, but since there is no curvature in 1D there is no surface-tension-like term analogous to the 2D case to counteract this growth when the applied field is sufficiently weak.

VI. DISCUSSION

In this section we discuss the applicability of our simulation results to switching in real SSFLC cells. The basic experimental observation is that electric field reversal nucleates many domains (although not necessarily all at the same time) which grow independently until they collide and coalesce. The morphology of these domains has several main features: (1) The domains are anisotropic, being elongated along the smectic layer direction and having flat or lightly rounded sides; (2) the back and front of the domains look different and grow with different speeds; they may also be faceted; (3) as the driving voltage is increased, the front-back asymmetry of the domains is reduced and they become more elliptical in shape.

In our simulations we have considered the growth of a single domain from an isolated nucleus. By introducing anisotropy in the elastic constants, domain growth is seen to occur more rapidly along the layers than perpendicular to them. Including a chevron binding potential leads to a flattening of the sides of the domain. However, there is evidently nothing in the present model to cause faceting or asymmetric growth in the layer direction.

Indeed, there is no obvious structural asymmetry of the Sm-C director field itself as derived from a purely elasto-electric free energy that breaks reflection symmetry. Essentially, only terms linear in $\nabla\phi$ (or in y or z) that appear in the equation of motion could produce asymmetric domains. Flexoelectric terms, which would qualify in principle, are estimated to be negligibly small [7]. The linear gradients describing spontaneous twist and bend of the ferroelectric polarization that appear in the full free-energy expression of FLCs [8] do not appear explicitly in the Euler-Lagrange equation (since they are boundary terms) and do not therefore affect the dynamics of reorientation.

There is an inherent asymmetry in the *layering* due to the chevron structure that may cause some difference in growth rates along the layer normal: the side of boat domains that grows toward the chevron apex is observed in some experiments to be shorter than the other side [7]. The observed front-back domain asymmetry, on the other hand, could result from the coupling of the director reorientation to flow, as proposed by Xue and Clark [7]. Preliminary calculations suggest that the inclusion of hydrodynamic effects would indeed introduce terms with the "correct" asymmetry into the equation of motion, and that such terms would tend to be more important at low fields [21]. This would be consistent with the observation that boat domains do become more symmetric in higher fields.

A. Domain collapse in zero field

Our simulations do reproduce, at least qualitatively, several features of SSFLC switching observed experimentally. For example, the computed velocity of domain walls is found to be proportional to E, as was discussed earlier. Experiments show that when domain growth is rapid the domain form is polygonal: if the applied field is then reduced so that the growth becomes slow (or stops completely) then the domains become rounded. If the field is reduced further, some domains (typically those below a certain size) will shrink and vanish. By comparison, computer simulations of domain dynamics confirm that domains of *any* size become rounded and shrink to nothing in the absence of an electric field, as illustrated in Fig. 9. While initially circular domains retain their form during this process, a domain in the form of a faceted ellipse shrinks anisotropically: when the field is first removed the domain shrinks primarily along its length (i.e., parallel to the smectic layers); only once the faceted sides have disappeared and the domain form is approximately elliptical does the domain start shrinking in the layer-normal direction as well. It is evident from Fig. 9 that, aside from an initial transient in the dynamics of the diamond-shaped domain, the domains all shrink linearly in time, at a rate that is independent of starting shape or size.

This time dependence may be estimated analytically for the case of a circular domain with isotropic elasticity K. If we ignore the effects of the chevron binding potential, then the rate at which the domain shrinks is governed by the balance of the release of elastic energy and viscous dissipation.

We consider a domain of radius R and wall width w, as shown in Fig. 10, shrinking at a steady rate. The polarization azimuth is assumed to be uniform everywhere except in the wall, where it changes linearly through an amount $\Delta\phi = \phi_2 - \phi_1$. Since the viscous torque density is $\Gamma = \eta\phi_t$ [cf. Eq. (2)], the rate of energy absorbed in the wall (per unit height) is

$$\frac{dW}{dt} = \int \frac{\eta\phi_t^2}{2}\, dA = \int \frac{\eta\phi_t^2}{2} 2\pi R\, dR.$$

Since the time derivative can be expressed as

$$\phi_t = \frac{d\phi}{dR}\frac{dR}{dt} = (\nabla\phi)\dot{R}$$

the integral can be written as

$$\frac{dW}{dt} = \int \frac{\eta(\nabla\phi)^2}{2}\dot{R}^2 2\pi R\, dR$$
$$\approx \frac{\eta}{2}2\pi(\nabla\phi)^2\dot{R}^2 Rw,$$

where we have assumed $w \ll R$. If we equate this quantity to the elastic energy released per unit time as the domain contracts, we have

$$-\frac{K}{2}(\nabla\phi)^2 w 2\pi\dot{R} = \frac{\eta}{2}2\pi(\nabla\phi)^2\dot{R}^2 Rw,$$

which simplifies to

$$\dot{R}R = -\frac{K}{\eta}.$$

This means that the area changes as

$$\frac{dA}{dt} = -\frac{2\pi K}{\eta}.$$

That is, the area of a circular domain decreases linearly in time. Interestingly, our simulations indicate that even initially cigar- or diamond-shaped domains acted on by the chevron binding potential also shrink linearly.

B. Domain stability in a stepped field

A fundamental question arising from experimental observations concerns the stability of domains of particular size in a given electric field: do they grow or shrink? Sustained domain growth over some time is clearly necessary to "latch" the SSFLC into a new polarization state. Although the general case of anisotropic chevron domains in arbitrarily varying electric fields is probably best dealt with numerically, we can perform a stability analysis analytically for the simpler case of an idealized circular domain with isotropic elasticity K and an E field changing in a stepwise manner. The domain has radius R and wall width w, as before.

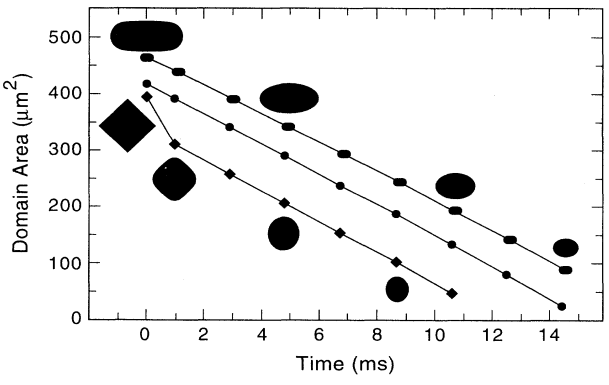

FIG. 9. Plot showing the area of domains vs time in the absence of applied field. The evolution is shown for three different starting shapes. These are, from top to bottom, (a) a steady-state faceted ellipse obtained in an applied field; (b) a circular domain; and (c) a diamond-shaped domain. The inset figures show the shapes at selected times for (a) and (c). The initial evolution of the diamond-shaped domain is relatively rapid, presumably because of the high energy associated with its sharp corners. For all three starting shapes, the dependence at long times is linear, i.e., $A \propto -t$.

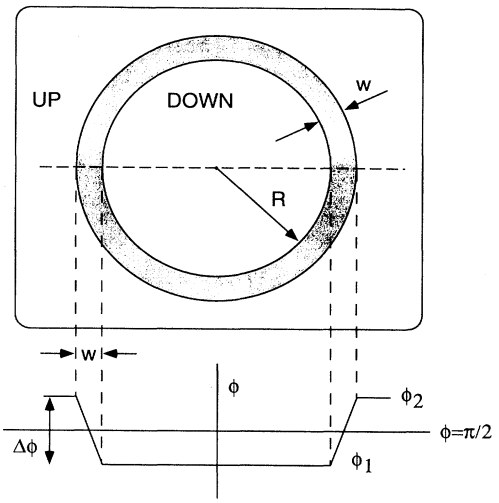

FIG. 10. Schematic diagram showing idealized circular domain structure used in effective surface tension calculation. The domain has radius R and wall width w. The polarization field inside the domain is down ($\phi = \phi_1$), outside it is up ($\phi = \phi_2$), and in the wall it changes linearly with a gradient $\Delta\phi/w$.

In general, the width of a domain wall is a function of applied field. In the case of a straight (1D) domain boundary, the wall becomes narrower with increasing E field, and broadens when the field is reduced, the width varying as $w \propto \xi$. In the absence of the chevron potential, if the field were removed the wall would expand as much as possible to reduce its elastic energy $\int(\nabla\phi)^2 dx$. The chevron term acts to limit the broadening because this process distributes molecules which are in unfavorable chevron orientations over a greater distance, raising the potential energy of the system. The equilibrium wall width is one that balances the elastic and chevron energy contributions.

We now consider the stability of a circular domain when the applied field strength is changed rapidly to a different value, as may be the case when a SSFLC is switched by short voltage pulses. Our analysis assumes that changes in wall width can initially be neglected. This theory cannot make detailed predictions about the behavior at longer times, or what happens if the field is changed slowly.

For the sake of clarity, we initially omit the chevron binding potential, and calculate the energy increase (per unit height) dW when the domain radius increases from R to $R + dR$. This is

$$dW = \frac{K}{2}(\nabla\phi)^2 2\pi w\, dR - PE\cos(\phi)\, 2\pi(2R + w)\, dR\,. \tag{8}$$

We see from the form of this equation that the Frank elasticity of the curved domain wall resists domain growth in the manner of a line tension of effective strength $\gamma_{\rm eff} = K(\nabla\phi)^2/(2wR)$. Since $\gamma_{\rm eff}$ falls off as $1/R$, we would expect the elasticity to dominate the response of small domains, but become less important as R gets large. The energy vs R curve is parabolic, with a maximum at

$$R_m(E) = \left(\frac{K}{2PE}\frac{(\nabla\phi)^2}{\cos\phi_1} - 1\right)\frac{w}{2} . \tag{9}$$

R_m thus corresponds to a condition of unstable equilibrium.

Now consider a domain of radius R undergoing steady growth in a field E_0, i.e., $R > R_m(E_0)$. At time t_1 the field is reduced rapidly to E_1. The new turning point immediately after field reduction is

$$R'_m(E_1) = R_m(E_0) + \left(\frac{E_0}{E_1} - 1\right)\frac{\xi_0^2}{2}\frac{(\nabla\phi)^2}{\cos\phi_1}\frac{w_0}{2} , \tag{10}$$

where $\xi_0 = (K/PE_0)^{1/2}$ is the field correlation length that determined the original domain shape. After the domain wall has readjusted its width from w_0 to w_1 the critical radius increases somewhat, and is given by

$$R_m(E_1) = \left(\frac{E_0}{E_1}\frac{\xi_0^2}{2}\frac{(\nabla\phi)^2}{\cos\phi_1} - 1\right)\frac{w_1}{2} . \tag{11}$$

Whether the domain now shrinks or continues to grow depends on the relative magnitudes of R and $R_m(E_1)$. If $R < R'_m(w_0)$ then the domain will definitely shrink and disappear. If, on the other hand, $R > R_m(w_1)$ then the domain will continue to grow. The behavior for intermediate values of R is difficult to predict. The stability conditions are sketched in Fig. 11.

The chevron potential $-(\gamma_4\cos\chi)/\ell$ introduced in Sec. III needs, to first order, only be considered in the wall region, the displacements from equilibrium in the rest of the sample being small in moderate electric fields. The additional contribution to the wall energy has the form

$$W_\chi = -2\pi R\frac{\gamma_4}{\ell}\int\left[C_0 + C_1\sin\phi - C_2\sin^2\phi\right]dR ,$$

where $C_0 = \cos 2\delta\cos^2\psi_0 + \sin^2\psi_0$, $C_1 = \sin 2\delta\sin 2\psi_0$, and $C_2 = -(\cos 2\delta + 1)\sin^2\psi_0$. After integration this yields

$$W_\chi = -2\pi R\frac{\gamma_4}{\ell}\left[C_0 w - \frac{1}{\nabla\phi}\left(2C_1\cos\phi_1 - \frac{C_2}{2}(\Delta\phi + \sin 2\phi_1)\right)\right] . \tag{12}$$

We note that this corresponds to the area contained below the potential barrier at $\phi = \pi/2$ shown in Fig. 4, so that $W_\chi > 0$. The change in this energy when R increases to $R+dR$ can be found by a trivial differentiation

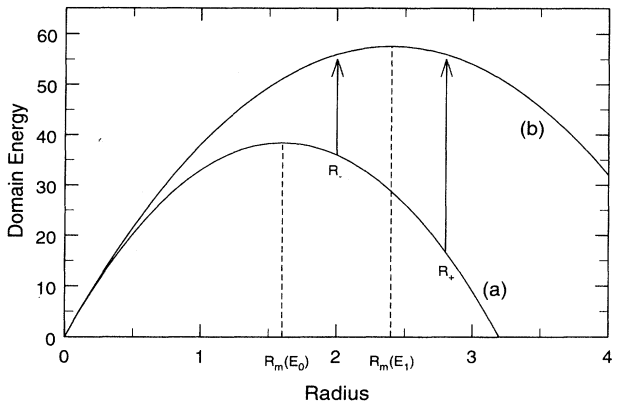

FIG. 11. Stability diagrams for circular domains. Parabola (a) describes the energy of a domain in a field E_0 as a function of radius R: if $R > R_m(E_0)$ then the domain grows without limit. At time t_1 the field is suddenly reduced to E_1, giving the new potential shown as curve (b). If $R > R_m(E_1)$ then the domain will continue to grow, otherwise it will shrink. For example, a domain with initial radius $R = R_+$ will grow while one with $R = R_-$ will shrink. The axes are scaled in arbitrary units.

of this equation to be $dW_\chi = (W_\chi/R)\,dR$. The complete energy differential is now [cf. Eq. (8)]

$$dW = \frac{K}{2}(\nabla\phi)^2 2\pi w dR - PE\cos(\phi)2\pi(2R + w)dR + dW_\chi ,$$

and the energy maximum is now at [cf. Eq. (10)]

$$R_m = \left(\frac{E_0}{E_1}\frac{\xi_0^2}{2}\frac{(\nabla\phi)^2}{\cos\phi_1} - 1 + \frac{1}{PE\cos\phi_1}\frac{W_\chi}{R}\right)\frac{w}{2} .$$

This critical radius is therefore somewhat higher than without the chevron term, i.e., higher fields are now necessary to ensure the continued growth of a given domain.

By varying the size of the initial nucleus, we have numerically determined the threshold field for growth as a function of domain radius using the full 2D model. The results, shown in Fig. 12, have the functional dependence predicted by Eq. (9). Corresponding experimental data have not yet been obtained and it remains to be established whether there is in fact an observable threshold field for domain growth (as distinct to domain nucleation) in chevron SSFLCs.

C. Domain nucleation dynamics

Finally, we address the question of how our numerical simulations, in addition to lending basic insight into the mechanisms of chevron SSFLC switching, can be used to help predict the electro-optic response of these cells. Since the optical transmission is a macroscopic property averaged in general over many domains, a calculation of the electro-optic response requires models for both the nucleation dynamics (density and rate) and the growth rate (area vs time) of individual domains. The long-time dynamics are complicated by the fact that many domains

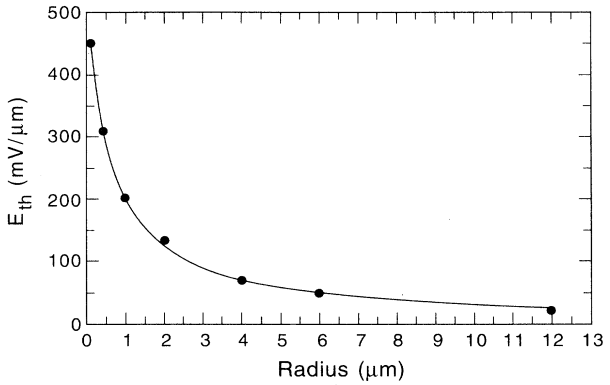

FIG. 12. Plot showing the threshold field for domain growth vs radius. The solid curve is a fit of the form $R = (a/E_{th} - b)$ [cf. Eq. (9)].

are generated during a typical switching event, so that collisions with neighboring domains occur and must be accounted for.

The nucleation dynamics have been discussed by Handschy and Clark [6], and Orihara and co-workers [12], and by Xue and Clark [7], who found that the experimental data can be fitted for the case of homogeneous nucleation by an Avrami law, with the fractional area with down polarization increasing as $A/A_0 = 1-\exp[-(t_1-t)]$ [12].

VII. CONCLUSION

In practice, comparisons of the model growth dynamics with experiments on SSFLC are complicated by inhomogeneities which occur in real cells, such as irregularities caused by spacer particles, layering defects (such as zigzag walls and boat wakes), and chemicophysical variations of the cell surfaces (such as rubbing and impurity effects). These may act to change the threshold voltages for domain nucleation and growth unpredictably, or serve as pinning sites impeding growth. For example, the experimental observation mentioned above, that some domains do not disappear when the field applied to the cell is reduced to zero, is behavior not explicitly accounted for by our model.

Nevertheless, a systematic comparison of experimental and numerical data should enable the determination of some physical parameters. For example, an inversion of the Wulff construction should yield the ratio of the Frank elastic constants. Measurements of threshold fields and switching times may yield an estimate of the chevron binding energy, γ_4.

ACKNOWLEDGMENTS

This work was supported by NSF Grants No. EEC 90-15128 and No. DMR 92-24168, and by ARO Contract No. DAA H04-93-G0164.

[1] R. B. Meyer, L. Liebert, L. Strzelecki, and P. Keller, J. Phys. (Paris) Lett. **36**, L69 (1975).
[2] N. A. Clark and S. T. Lagerwall, Appl. Phys. Lett. **36**, 899 (1980).
[3] T. P. Rieker, N. A. Clark, G. S. Smith, D. S. Parmar, E. B. Sirota, and C. R. Safinya, Phys. Rev. Lett. **59**, 2658 (1987).
[4] J. E. Maclennan, M. A. Handschy, and N. A. Clark, Liq. Cryst. **7**, 787 (1990).
[5] J. E. Maclennan, N. A. Clark, M. A. Handschy, and M. R. Meadows, Liq. Cryst. **7**, 753 (1990); Z. Zhuang, N. A. Clark, and J. E. Maclennan, *ibid.* **10**, 409 (1991).
[6] M. A. Handschy and N. A. Clark, Appl. Phys. Lett. **41**, 39 (1982).
[7] J.-Z. Xue and N. A. Clark, Phys. Rev. E **48**, 2043 (1993).
[8] M. A. Handschy and N. A. Clark, Ferroelectrics **59**, 69 (1984).
[9] Y. Ouchi, H. Takezoe, and A. Fukuda, Jpn. J. Appl. Phys. **26**, 1 (1987); Y. Ouchi, H. Takano, H. Takezoe, and A. Fukuda, *ibid.* **27**, 1 (1988); N. Hiji, Y. Ouchi, H. Takezoe, and A. Fukuda, *ibid.* **27**, L1 (1988).
[10] S. Nonaka, K. Itoh, M. Isogai, and M. Odamura, Jpn. J. Appl. Phys. **26**, 1609 (1987).
[11] Y. Yamada, T. Tsuge, N. Yamamato, M. Yamawaki, H. Orihara, and Y. Ishibashi, Jpn. J. Appl. Phys. **26**, 1811 (1987); Y. Ishibashi, H. Orihara, K. Nakamura, and Y. Yamada, *ibid.* **26**, 107 (1987).
[12] See H. Orihara, Y. Ishibashi, and Y. Yamada, J. Phys. Soc. Jpn. **57**, 4101 (1988); Y. Yamada, N. Yamamoto, T. Inoue, H. Orihara, and Y. Ishibashi, Jpn. J. Appl. Phys. **28**, 50 (1989); and extensive references therein.
[13] N. A. Clark and T. P. Rieker, Phys. Rev. A **37**, 1053 (1988).
[14] Z. Zhuang, J. E. Maclennan, and N. A. Clark, in *Liquid Crystal Chemistry, Physics, and Applications*, edited by J. William Doane and Zvi Yaniv [Proc. SPIE **1080**, 110 (1989)].
[15] J. E. Maclennan, M. A. Handschy, and N. A. Clark, Phys. Rev. A **34**, 3554 (1986); J. E. Maclennan, N. A. Clark, and M. A. Handschy, in *Solitons in Liquid Crystals*, edited by Lui Lam and Jacques Prost (Springer-Verlag, New York, 1992).
[16] See, for example, G. D. Smith, *Numerical Solutions of Partial Differential Equations: Finite Difference Methods*, 2nd ed. (Clarendon, Oxford, 1978); B. Carnahan, H. A. Luther, and J. O. Wilkes, *Applied Numerical Methods* (Wiley, New York, 1969).
[17] G. Wulff, Z. Kristallogr. **34** 449 (1901).
[18] C. Herring, Phys. Rev. **82**, 87 (1951); in *Structure and Properties of Solid Surfaces*, edited by R. Gomer and C. Smith (University of Chicago Press, Chicago, 1953).
[19] J. Rudnick and R. Bruinsma, Phys. Rev. Lett. **74**, 2491 (1995).
[20] Q. Jiang, J. E. Maclennan, and N. A. Clark (unpublished).
[21] Z. Zou, V. Ginzburg, J. E. Maclennan, and N. A. Clark (unpublished).

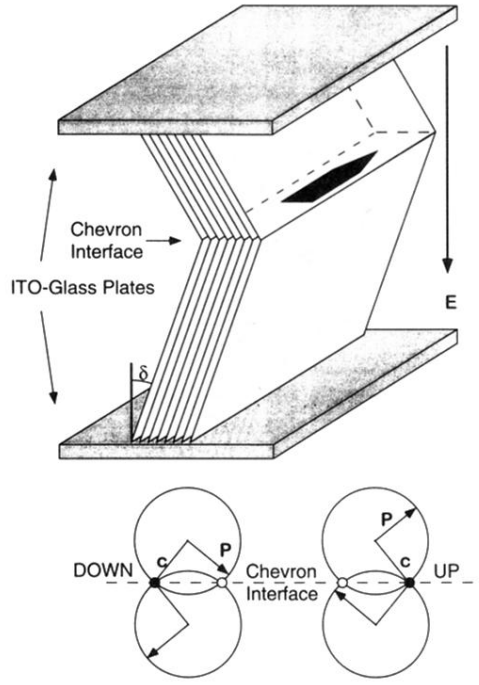

FIG. 1. Geometry of chevron SSFLC cell. The smectic layers are tilted an angle $\pm\delta$ from the cell normal, the change in their orientation typically occurring near the middle of the cell. The orientational binding potential at this planar chevron interface stabilizes two polarization states $\mathbf{P}$, up and down. The corresponding director orientations are indicated in the lower part of the figure by the filled circles ($\bullet$) and their projections onto the smectic layer planes by the c director ($\mathbf{c}$). A generic polygonal domain is shown growing at the chevron interface.

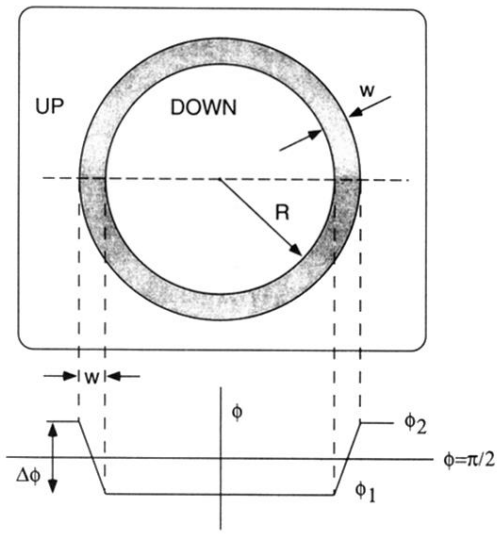

FIG. 10. Schematic diagram showing idealized circular domain structure used in effective surface tension calculation. The domain has radius R and wall width w. The polarization field inside the domain is down ($\phi = \phi_1$), outside it is up ($\phi = \phi_2$), and in the wall it changes linearly with a gradient $\Delta\phi/w$.

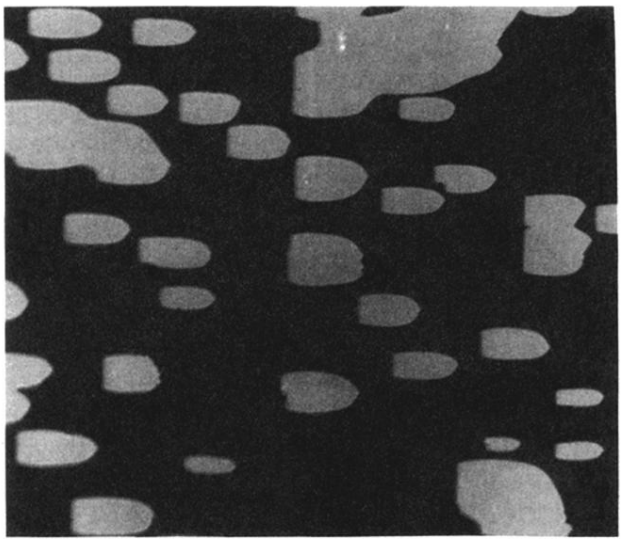

(a)

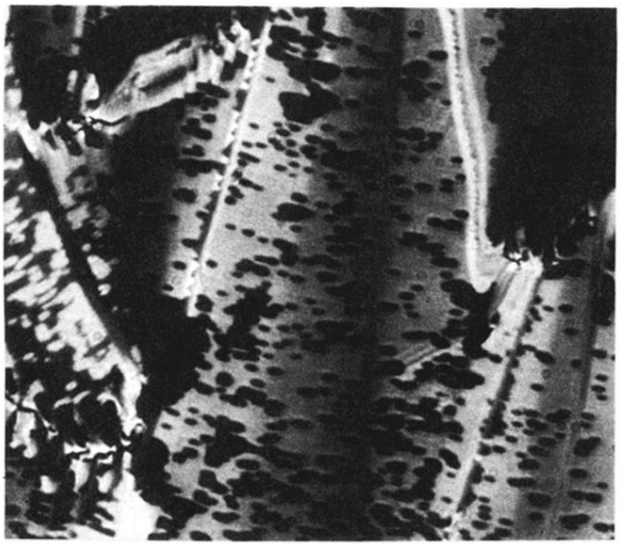

(b)

FIG. 2. Domain shapes in chevron SSFLC cells: (a) low-voltage switching in a 4 μm cell of the Merck material ZLI-3654. The domains are boat shaped, with gently rounded sides. The applied voltage is about 20 mV. (b) High-voltage switching in a 2 μm cell of the Displaytech mixture W7-W82. The picture, taken stroboscopically, shows rather symmetric domains growing about 3 ms after a field reversal. The applied voltage is 12 V. The layer normal is in both cases approximately vertical.

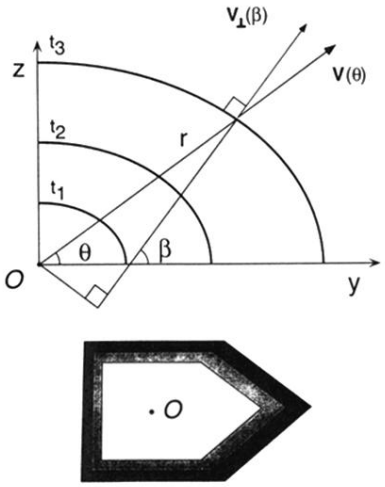

FIG. 5. Geometry of domain shape calculations. Part of a curved domain wall $r(\theta)$ is shown at different times t_1, t_2, and t_3. The radial domain wall velocity $v(\theta)$ is constant for a given θ. The local orientation of the domain wall along any radius vector is also constant in time so that the growth is self-similar. The construction relates the radial velocity to the normal component of the velocity $v_\perp(\beta)$, the latter being equal to the velocity of an infinite planar wall with the same orientation. The lower part of the figure shows a hypothetical five-sided boat domain growing in self-similar fashion: the pointed bow moves fastest and is furthest from the "origin" O.